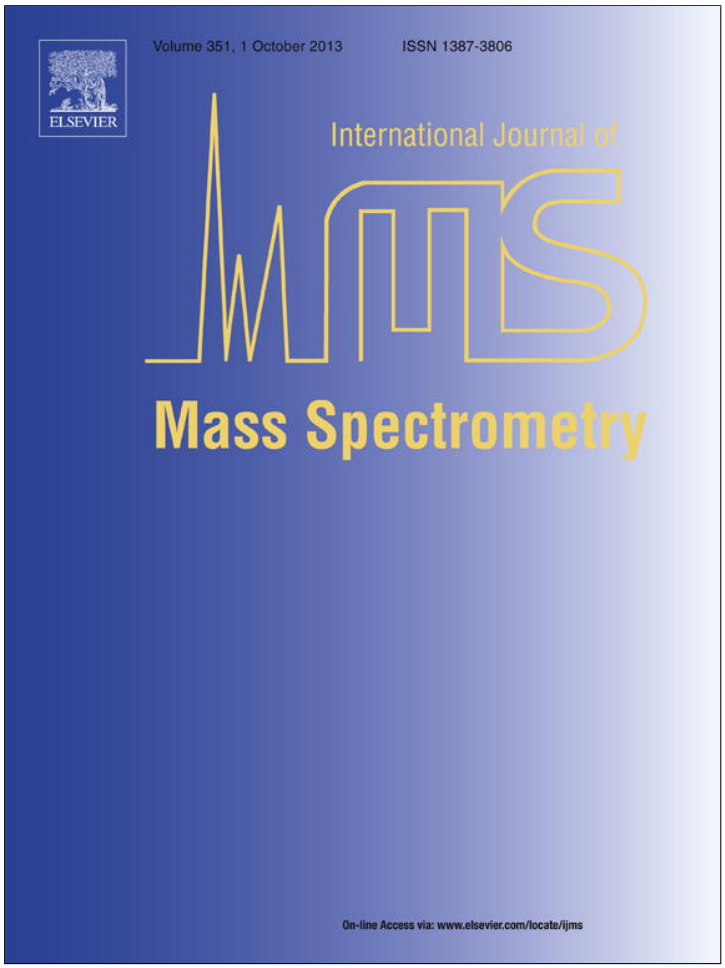

International Journal of Mass Spectrometry 351 (2013) 47–55

Contents lists available at ScienceDirect

International Journal of Mass Spectrometry

journal homepage: www.elsevier.com/locate/ijms

$Mg^+(^2S)$ and $Mg^+(^2P)$ in reaction with $H_2(^1\Sigma_g^+)$: A description of the energy surfaces explaining the mechanisms

M. Satta[a], M. Marquéz-Mijares[b], E. Yurtsever[c], S. Bovino[d], F.A. Gianturco[d,*]

[a] CNR-ISMN and University of Rome "Sapienza", P. le A. Moro 5, 00183 Rome, Italy
[b] Instituto de Fisica Fundamental, IFF-CSIC, Serrano 123, 28006 Madrid, Spain
[c] Department of Chemistry, Koc University, Rumelifeneri Yom, Sariyer, 34450 Istanbul, Turkey
[d] Department of Chemistry, "Sapienza" University of Rome, P. le A. Moro 5, 00185 Rome, Italy

ARTICLE INFO

Article history:
Received 6 February 2013
Received in revised form 25 March 2013
Accepted 25 March 2013
Available online 27 June 2013

Keywords:
Ion-molecule reactions
Potential energy surface calculations
non-adiabatic coupling calculations

ABSTRACT

The lowest two potential energy surfaces which involve $Mg^+(^2P)$ and $Mg^+(^2S)$ atoms interacting with H_2 molecules are computed to describe both the intermediate complex $[MgH_2^+]$ formed during their reactive approaches and the asymptotic outcomes of $MgH^+ + H$ or of $Mg^+ + H_2$. The calculations clearly reveal the presence of an avoided crossing between the two surfaces near the T-geometry of the complexes and the existence on the upper surface of regions where the ionic atomic states of magnesium are "coordinated" with either $H_2(^1\Sigma_g^+)$ or $H_2(^3\Sigma_u^+)$ states. The implications of these structural results with respect to the existing experiments in cold ion traps are discussed and shown to provide already a qualitative explanation for the final formation of MgH^+/MgD^+ ions in the trap. In fact, a simplified treatment of the nonadiabatic coupling effects in the region of closest approach between the two Born–Oppenheimer surfaces is given via Landau–Zener curve crossing models and are found to already yield a realistic picture of the behavior seen by the experiments.

1. Introduction

Very impressive progress has been made over the last few years with the preparation and control of the internal quantum states of molecules with translational energies down to temperature values of $T \ll 1$ K [1–5]. Thus, neutral diatomics produced from ultracold atomic gases have been obtained in specific rotational, vibrational and even hyperfine internal states, while similar efforts have also been undertaken to control the internal states of translationally cold molecular ions in traps, where their translational motion can be cooled sympathetically by using Coulomb interactions between simultaneously trapped, laser-cooled atomic partners [6,7]. Using such methods, therefore, translational temperatures in the milliKelvin regime can be achieved, so that the ions localize in the trap to form ordered structures known as "Coulomb crystals" [8].

One should be reminded, however, that in contrast to buffer-cooling methods in cryogenic traps [9], the above sympathetic cooling approach does not affect the internal degrees of freedom of the trapped molecular ions, which therefore remain internally warm and are usually in thermal equilibrium with the ambient black-body radiation [10]. These studies have thus shown that a fairly large number of molecular ions, e.g. MgH^+ and MgD^+ [6], can be formed translationally very cold ($T < 100$ mK) by photochemical reactions and then sympathetically cooled in linear Paul traps using the Coulomb interaction with laser-cooled Mg^+ ions [11]. The chemical reaction employed was [6]

$$Mg^+(3p^2P_{3/2}) + HD \rightarrow MgH^+/MgD^+ + D/H \quad (1)$$

monitored in the trap by following the radial separation of ions with different charge-to-mass ratios. The isotope effects were further investigated and the branching ratio between formation of MgD^+ and MgH^+ was found to be larger than 5 [12].

Because of the fairly simple internal structure of the reaction partners, the process depicted in (1) could provide an interesting test case for the studies of reaction dynamics involving the role of electronically excited partner ions. It is therefore of importance to see how far a computational analysis of the interaction forces can help us in understanding the actual nanoscopic mechanisms of the above reaction, even before an analysis of its quantum dynamics.

In the experiments [12] the isotope effects in reaction (1) was analysed by considering reactions at thermal energies with Mg^+ in its $3p^2P_{3/2}$ excited state (with an excitation energy of 4.4 eV [12]). The reacting $^{26}Mg^+$ ions were loaded into a linear Paul trap [13] by crossing an effusive beam of Mg atoms with a laser beam at 285 nm in the trap center, thereby forming $^{26}Mg^+$ ions by two-photon, resonance-enhanced ionization of the neutral atom [12]. The resulting ions were further Doppler laser cooled using the

* Corresponding author. Tel.: +39 0649913306.
E-mail address: francesco.gianturco@uniroma1.it (F.A. Gianturco).

1387-3806/$ – see front matter © 2013 Published by Elsevier B.V.
http://dx.doi.org/10.1016/j.ijms.2013.03.019

$3p^2P_{3/2} \leftarrow 3s^2S_{1/2}$ transition, so that individual ions can be observed by light imaging during the cooling process.

Reactions with HD, H_2 or D_2 were investigated by leaking the above gases in the trap chamber and then uploading two $^{26}Mg^+$ ions into it: only reactions with the excited electronic state of the ion are seen to occur, since the corresponding reactions with Mg^+ ($3s^2S_{1/2}$) ground state configurations are energetically forbidden [6]. The formed molecular species is then kept in the trap and, within tens of ms, sympathetically cooled through Coulomb interactions with the residual (laser cooled) $^{26}Mg^+$ ions, thereby forming a two-ion Coulomb crystal [12]. The chemical reaction was also found to display a remarkable isotope effect related to the molecular reactive mechanism (to be discussed below), and the suggestion from the experimental work [12] was that it occurred as a two step mechanism whereby the neutral molecule (H_2, HD or D_2) is first captured in the trap by the $^{26}Mg^+$ ion as a long-range structure, thus forming MgH_2^+ or $MgHD^+$ as an intermediate collision complex. As a second step, the final molecular ion MgH^+ or MgD^+ is formed by complex rearrangement and break-up in the short-range region of the interaction [12].

The structural study which we are reporting in the present work is therefore investigating such a two-step process by analysing the spatial behaviour of the two adiabatic electronic surfaces which asymptotically connect with the ground and excited states of the partner atomic ion Mg^+ (^2S or ^2P mentioned earlier) and see what information could be gathered on at least three crucial questions:

- do calculations find a complex-formation stage, indicating a two-step mechanism as suggested by the experiments?
- could this complex formation provide a link with the observed strong isotopic effects in this reaction?
- what is the role played by the upper electronic potential energy surface in producing the reaction products?

The paper is organized as follows: the next section briefly describes the computational method and the details of the reactive potential energy surfaces (RPES), while Section 3 discusses the overall topology of what we find over the two adiabatic surfaces. The simple nonadiabatic modelling of the coupling is reported in Section 4, while our conclusions are presented in Section 5.

2. Computational details

The electronic structure method employed to get the RPES is complete active space (CAS) with 3 electrons in 8 active molecular orbitals; namely the 3s and the 3p of Mg, and the 1s and 2s of H as calculated by ROHF at the initial geometry of the scanning procedure. At each of the selected geometries the initial wavefunction was from the CASSCF computation of the previous nearest geometrical point. Five core orbitals (doubly occupied and fully optimized) were chosen for the complex of MgH_2^+, and six of total CI states have been computed. The inclusion of four excited state, beyond the ground and the first excited state, provides a proper treatment of the interaction among the first excited state and the second excited state, as found by Bauschlicher [15]. The orbital optimization step followed a second order method, with an exact orbital hessian. In order to improve numerical stability, the energy of the first excited electronic state have been obtained by mixing 1% of the ground state configuration with 99% of the second energy level, and a tolerance of 10^{-10} au on the energy was chosen. The C_s symmetry was imposed on the electronic calculations, and the Dunning-type correlation consistent basis sets was used with level three of polarization (aug-cc-pvtz). The parameters used for the two RPES are the two Mg–H distances and the H—Mg—H angle. The Mg—H distances are irregularly distributed in the range 1.5–9.0 Å, and the angle H—Mg—H varies from 0 to 180°, so that a total of 18174 points have been used. The RPES of the linear-shape and T-shape have been built considering also the optimization of the H—H bond and distance between Mg and the center of mass of H_2. The counterpoise procedure has been employed to estimate the Basis Set Superposition Error (BSSE) in the region of the crossing. The GAMESS [14] program was employed to obtain all the present data.

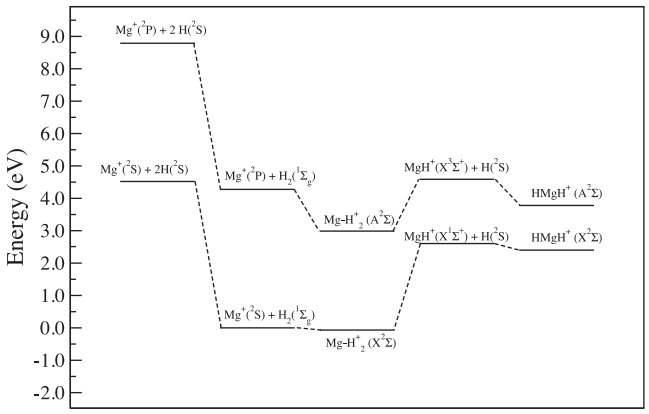

Fig. 1. Computed asymptotic energy levels of the various arrangements discussed here for the $(MgH_2)^+$ electronic states relevant for the reaction observed in cold traps. See main text for further details.

3. Discussing the topology of the two RPESs

The large number of RPES points generated for both the lower and upper potential surfaces indicate regions of geometries close in energy but no clear crossing seams. Since such reductions of the energy gap are particularly significant for the T-shape and linear-shape complexes for $(MgH_2)^+$ partners, it is important to first establish the asymptotic energy relations which exist among reacting species. Furthermore, since the experimental studies suggest a complex-formation step during the evolution to molecular ions as products [12], it is also important to clarify such preferential structures among partners.

3.1. The involved asymptotic states

The data of Fig. 1 provide an overall view of the various energy levels of the complex system on the two RPESs. At the extreme left we show the locations of the three-body (3B) break-up states of the total complex for the two electronic states discussed in this work: their energy difference includes both the ($3p \leftarrow 3s$) atomic excitation energy and the D_0 of the $H_2(X^1\Sigma_g^+)$ molecule in its ground roto-vibrational state. Next to them we show energy difference between ionic states: it corresponds to about 4.34 eV of excitation energy.

The optimized-geometry energy levels for the two T-shaped complex structures are reported next, further right in the same figure. One clearly appreciates the marked difference of stabilization energies between the two complex structures: one weakly bound of $Mg^+(3s)$ with $H_2(^1\Sigma_g^+)$ and one much more strongly bound for excited $Mg^+(3p)$ with $H_2(^1\Sigma_g^+)$.

The asymptotic energy levels of the two channels leading to MgH^+ formation from the two RPESs are reported next, always to the right of the previous data: they clearly show that the formation reaction on the lower RPES is strongly endothermic while the endoergic process on the upper surface requires about 0.13 eV less energy. The molecular ion formed is, however, in its $X^3\Sigma^+$ state which is only very weakly bound and therefore not likely to survive in the trap. The last set of data on the extreme right of Fig. 1

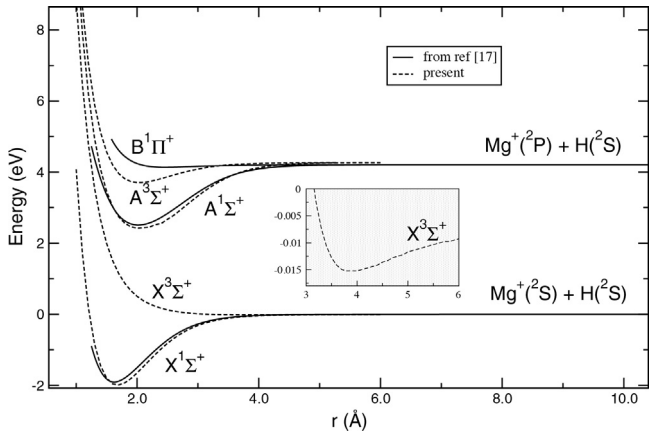

Fig. 2. Computed potential energy curves for the electronic states of isolated MgH^+ partner relevant for the present study. See text for further details.

report the relative energy positioning of the insertion, linear complexes on both RPESs. On stretching the H—H on the lower surface the linear complex provides an interesting intermediate configuration for the evolution of the present system. On the other hand, the same complex on the upper RPES undergoes a less marked excitation with respect to the stable, T-shape complex, indicating the weaker deformation of the "singlet" structure with respect to that found on the lower RPES.

The potential energy curves for that lower electronic states of MgH^+ are given by Fig. 2. The data show that the present level of calculation compares well with the multi-reference study done earlier on the same system [20], while also showing the marked energy gain obtained in forming $MgH^+(^1\Sigma^+)$ in the lower RPES in comparison with the $MgH^+(X^3\Sigma^+)$ formed on the upper surface: this means that its formation on the lower surface causes a gain which can easily be converted into relative translational energy of the residual H/D atom leaving the complex after break-up. What the relative positioning of the various states of the complex given in Fig. 1 also shows is the proximity in energy between the $(Mg–H_2)^+$ complex on the excited RPES and the asymptotic products of the reaction, the $MgH^+(X^1\Sigma^+)$ and the $H(^2S)$ residual atom, given by the lower surface. It is therefore this down-transition from the upper surface that provides the second step (after the upper complex formation) of the title reaction, as we shall further discuss after providing below detailed information on the general features we found for the reacting species on the two coupled RPESs.

3.2. The T-shaped complex on the lower surface

An earlier study [15] carried out an analysis of the ground and low-lying states of MgH_2^+ using complete active space self-consistent field and multireference configuration interaction. They found a T-shape configuration to be the dominant structure for the bound complexes, with the X^2A_1 ground state fairly weakly bound by 0.095 eV while the next excited-states, the $^2B_2$ and $^2B_1$ turned out to be more strongly bound (1.973 and 0.798 eV, respectively) and to undergo strong bond deformations: the Mg^+ distance from the H_2 mid-point is, in fact, around 5 a_0 for the $^2A_1$ and about 2.6 a_0 for the $^2B_2$, while the H_2 distance changes from 1.4 a_0 to 4.4 a_0. Thus, one could say that the insertion path of Mg^+ in its 3p-state generates a much stronger bonding with H_2 while forcing the partner molecule to acquire a much more stretched bond within the complex [15]: our present calculations agree well with the above findings, while the fact that our present calculations indeed sample the two relevant electronic surfaces over a much more broad range of configurational points than in the previous work will help us in shedding more light on the effects of the above features on the chemical process: they will also indicate a possible mechanism for the electronic evolutions after laser excitation of Mg^+ (3s).

A more recent computational study [16] provided a three-dimensional ground state potential energy surface (PES) to describe the structures of $Mg^+–H_2$ and $Mg^+–D_2$ complexes, i.e. only the lower of the PESs computed in the present work. From that study the authors found the fairly weak perturbation of the strong H_2/D_2 bonds caused by the ionic partner, confirmed by the present work where we indeed see that it forms with that molecule a T-shaped complex with a well depth of about 0.104 eV and a dissociation energy of 0.076 eV. This should be compared with the earlier value [16] of 0.0651 eV, where the distance between the ion and the mid-point of the H_2 bond was confirmed to be around 5 a_0, or 2.62 Å. A comparison between our results on the complex's structure in the T-shape geometry of the ground state and data from literature is provided in Table 1. Our binding energy is slightly smaller than [16], but the discrepancy can be ascribed to a partial neglecting of dispersive forces within our choice of basis set expansion, due to the much larger number of configurational points we need to generate in the present study. On the other hand, this partial neglecting of dispersive attraction effects should be of similar importance for both the ground and the excited electronic states, especially near the crossing seam that we are analyzing, as we shall further discuss below. The excited electronic surface, at variance with the ground PES, is characterized by a minimum energy geometry with a substantial decrease of the $Mg–H_2$ distance (−0.22 Å) and a corresponding increase in the H_2 bond length (+0.56 Å), in qualitative agreement with the data of Bauschlicher [15].

3.3. The ground state minimum energy path

It is now instructive to follow the minimum energy path (MEP) between partners on the lower RPES as a function of their relative orientations since such an analysis can help us to better understand both the location of the complex and the role of the upper RPES that is reached by laser excitation of Mg^+ (3p←3s).

The four panels reported in Fig. 3 describe such paths for the orientation angles defined in each of them in the upper right corners. The following comments could be made:

- the destruction of MgH^+ is a strongly exothermic reaction, so that the interaction between Mg^+(3s) and H_2 ($^1\Sigma_g^+$) will not lead to the formation of a molecular ion (as already discussed in the introduction) unless one deals with strongly internally excited H_2 partners, an option excluded in the trap experiments [12].
- the global system forms a weakly bound complex at shorter distances, as mentioned earlier. At orientations closer to the T-shape of the complex (60° and 90° degrees) the MEPs show a more marked attractive well (about 0.3 eV) with respect to quasi-linear orientations (about 0.2 eV). At $\theta = 180°$ there is no repulsive barrier to form the product MgH^+, whereas a barrier of about 0.2 eV is present in the non-linear cases;
- the existence of an upper surface containing the Mg^+(3p) species is hinted at by the avoided crossing effects near those barriers, indicating that the closest approach between the two surfaces is likely to happen in the neighbourhood of the T-shaped complex within each adiabatic surface: this feature will be further discussed below.

Another interesting feature of the lower RPES could be observed via the "insertion" path of the most stable complex, seen in the figure to occur around the T-shaped geometry [15,16]: the necessary stretching of the H—H bond causes a marked energy increase along this path, as clearly shown in the contour map of the lower RPES reported by Fig. 4.

Table 1
Minimum energy features of the ground state of MgH_2^+ in the T-shape geometry: comparison with previous calculations.

	CASSCF[a]	CASSCF/MRCI[b]	RCCSD(T)[c]	CASSCF/MRCI[d]	MP2[e]	IC-MRCI+Q[f]
R_{Mg-H_2} (Å)	2.90	2.72	2.62	2.67	2.72	2.65
D_e (cm^{-1})	540	769	842	771	416[g]	759
R_{H_2} (Å)	0.75	0.75	0.75	0.75	0.74	–

[a] Present results.
[b] [15] See there for basis set details. No BSSE correction.
[c] [16] H: aug-ccpVQZ, Mg: cc-pVQZ basis, a set of 3s3p2d2f1g bond functions centered between the Mg and the H_2. BSSE correction.
[d] [17] H and Mg: ANO. No BSSE correction.
[e] [18] H and Mg: aug-cc-pvtz. No BSSE correction.
[f] [19] H: aug-cc-pVQZ, Mg: ANO-RCC. BSSE correction.
[g] D_o value.

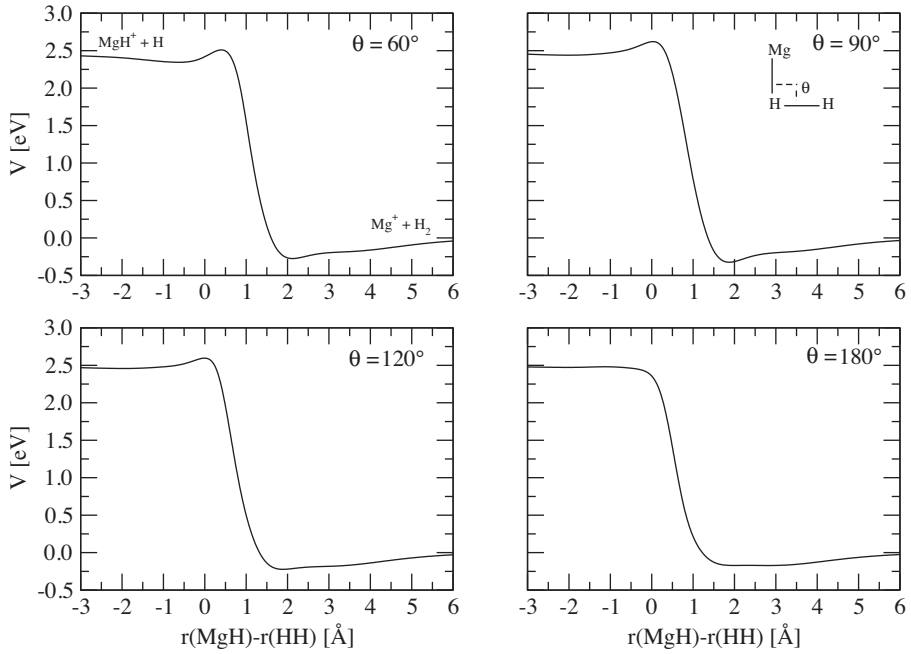

Fig. 3. Computed minimum energy paths in the lower RPES for four different values of the angle θ, defined in the upper right panel. Binding energies are: $D_e(90^\circ)$=0.32 eV, $D_e(60^\circ)$=0.27 eV, $D_e(120^\circ)$=0.22 eV, $D_e(180^\circ)$=0.17 eV.

The calculations of that figure show that when the $Mg^+(3s)$ distance from the H_2 midpoint goes to zero one observes a substantial increase of the H—H distance to about 3.30 Å, and thus the much more "stretched" H_2 bond occurs with an energy increase of more than 2 eV. One further characteristic of our calculations is obtained when one looks at the separate density distributions of the "α" and "β" spin states of the three electrons involved in the bonding: the formation of a linear complex within the ground state indicates that the two H atoms are in a "singlet" state of that molecular partner with "H_α" and "H_β" spin states of the two "atomic" electrons. We therefore see that the ionic $Mg^+(3s)$ state is bound within the complex to a "singlet" state of the partner hydrogen molecule, thereby leading to an energetically higher, local linear complex with a weak bond.

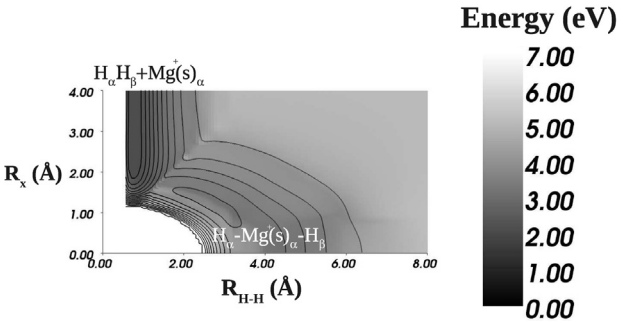

Fig. 4. Computed RPES in the T configuration for the electronic ground state. Distances in Å. The basin in the middle of the surface describes the weakly bound, excited complex with a nearly linear complex where Mg^+ is inserted into the H—H bond.

3.4. The T-shaped complex on the upper RPES

That the situation dramatically changes when the (3p←3s) excitation occurs for the magnesium ion, could be gathered from the behaviour of the upper RPES within the region of geometries for the T-shaped approach on the ground electronic state, reported by the contour map of that surface in Fig. 5. The panels shown in Fig. 3 for the ground state RPES had reported the energy paths defined by the two asymptotic channels, whereby on the right the system reaches its lowest energy content by forming $Mg^+(3s)$ +$H_2(^1\Sigma_g^+)$ molecules while, when moving on the left to larger H–H distances and smaller Mg–H_2 distances it produced the insertion complex discussed by Fig. 4 which contains H atoms in the opposite spin state, i.e. binding the $Mg^+(3s)$ to an internal "singlet" state of a markedly stretched H_2.

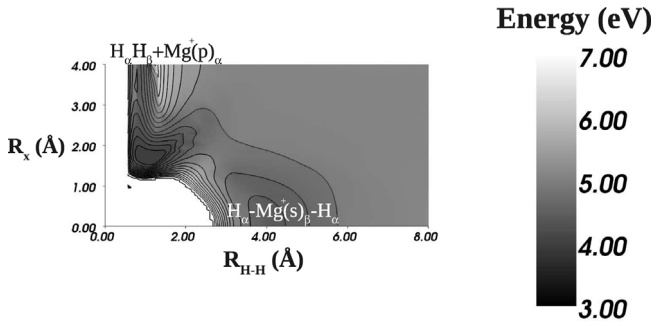

Fig. 5. Computed RPES for the T configuration of the previous figure but now on the electronic excited state. Distances in Å; energies in eV. See main text for further details.

This feature is now modified on the excited RPES of Fig. 5 where different regions could be seen as existing: (i) $Mg^+(3p)+H_2(^1\Sigma_g^+)$ at intermediate $Mg^+–H_2$ distances but fairly small H–H distances, thus forming that complex, (ii) over a small barrier, another T-shaped complex more stably bound and closer in geometry to the earlier calculations on the ground state RPES [15]: (iii) after a further small barrier there is yet another complex structure with the $Mg^+–H_2$ distance going to zero, i.e. Mg^+ insertion forming H-Mg^+(3s)–H with H–H in a "$^3\Sigma$" state, i.e. with the H_1^α and H_2^α spin states within the complex. In the region around the crossing seam at the T-configuration our calculations therefore show formation, along an exothermic path, of the ground state ion Mg^+(3s) with a dissociative H_2. That complex could further back-cross into the lower RPES and lead to Mg^+ bond formation with one H atom and to the other H atom release, as we shall further discuss below. The existence of such different features on the upper surface suggests that the Mg^+(3s) ion could exist on that PES within different triatomic complexes: one would be with a "triplet" state of the H_2 partner which is in a dissociative state within the complex and, by nonadiabatic crossing, it could return to the lower PES as we shall further discuss below.

3.5. Evolution of the H–Mg–H insertion complex

Another orientational choice for the two surfaces is reported by Fig. 6 to better clarify the present discussion. It corresponds to the Mg^+ approaching the H_2 molecule along the collinear path

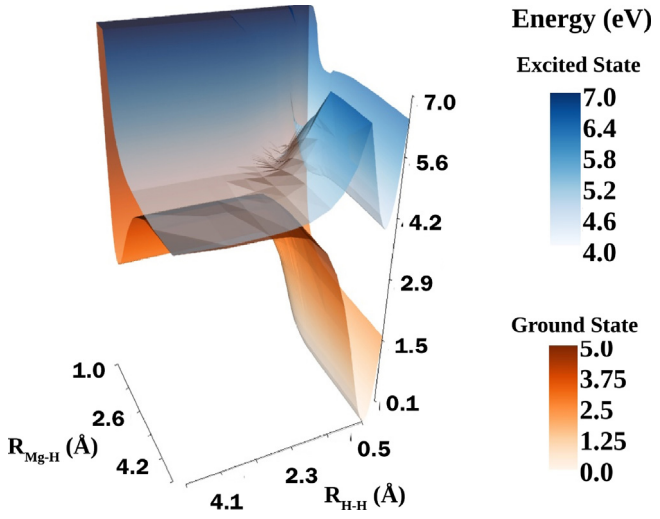

Fig. 6. Computed upper and lower RPESs for the linear configurations of the $(H_2$-$Mg)^+$ complexes on both surfaces. Distances in Å, energies in eV. See main text for further details.

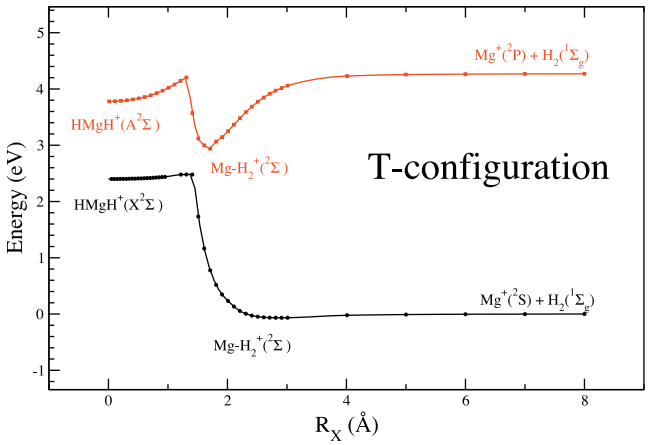

Fig. 7. Computed energy evolutions of the T-shape complex structures as a function of Mg^+ distance from bond mid-point of H—H. Lower curve: involving the Mg^+(3s) ion; upper curve: for the case of the Mg^+(3p) ion. The discontinuity in the excited state is due to a "crossing" between the state $[Mg^\alpha(p)H_2^{\alpha\beta}]^+$ at long range R_x with the state $[H^\alpha Mg^\alpha(s)H^\beta]^+$ at R_x less than 1.3. In the ground state at long range R_x the state $[Mg^\alpha(s)H_2^{\alpha\beta}]^+$ "crosses" with the state $[H^\beta Mg^\alpha(s)H^\beta]^+$ at R_x less than 1.3.

following both RPES with Mg^+(3s) and Mg^+(3p) ionic partners respectively. Some interesting features now highlight what we have already discussed before:

- the linear path on the ground state RPES shows, at shorter H—H distances and large Mg^+–H distances, the expected potential curve of the $H_2(^1\Sigma_g^+)$ state bound to the Mg^+(3s) state: as the distance between that ion and the H atoms is shortened, the corresponding H–H distance increases, as does the overall energy, reaching the MgH^+ +H break-up region of the molecular complex;
- at larger H–H distances the lower surface moves closer to the upper one, reaching from below the region where the Mg^+(3s) is formed in the presence of a repulsive H–H curve associated with the $(^3\Sigma_u^+)$ state: it is the same configuration discussed before where the Mg^+(3s) moves away from its partner molecule once the upper surface is reached;
- the upper RPES therefore shows two distinct regions with respect to the H–H distance: at shorter distances the Mg^+(3p) state is coupled to the $(^1\Sigma_g^+)$ state of the H_2 molecule so that the H–H curve within the complex, in both the upper and the lower REPS, is that of the bound molecular hydrogen. However, as the H—H bond stretches, at short Mg^+(3p)–H_2 distances there is a dissociating region where the system could fairly easily move to larger distances of the Mg^+ from the hydrogen molecule: the latter molecule evolves in turn into a repulsive H_2 molecule while the former into an Mg^+(3s) partner ion.

In conclusion, the data of Figs. 5 and 6 indicate that, once the initial T-shaped triatomic complex reaches the upper RPES during laser excitation, the Mg^+(3p) associated with the $H_2(^1\Sigma_g^+)$ could move adiabatically to a configurational region where it becomes Mg^+(3s) associated with a highly repulsive state of the $H_2(^3\Sigma_u^+)$.

3.6. Mapping the energy profiles of both complexes

A different presentation of what discussed thus far can be obtained by looking at the energy profiles depicted in Figs. 7 and 8 . What we wish to show there is the overall energy profiles which are followed by the present set of partners depending on their relative

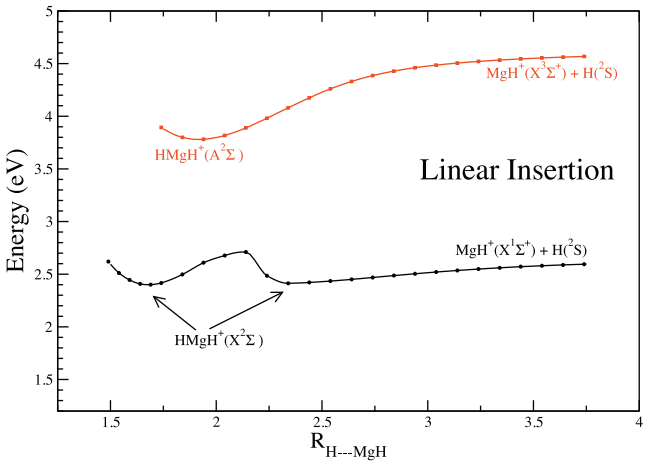

Fig. 8. Computed linear insertion geometries of the upper and lower RPESs, as a function of one $R_{H---MgH}$ distance, having optimized at each point the other Mg–H distance. See text for further details.

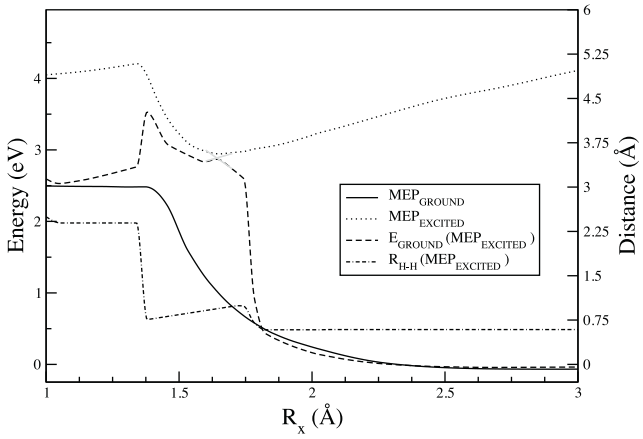

Fig. 9. Computed MEPs for the T-shape approach on both RPESs and as a function of the ion's distance from the mid point of the H–H optimized distance. See text for further details and explanations of the curves presented.

orientations and on the RPES which is being sampled during their motion. The evolution of the T-shape configuration is reported in Fig. 7. If one looks at the lower curve, the exothermic nature of the MgH^+ destruction process is clearly visible at the largest distances on the right, where the $Mg^+(3s)$ ion exists separately from the $H_2(^1\Sigma_g^+)$. As the distance is reduced we first see the formation of the weakly bound complex described in our previous figures and by the earlier calculations [15,16]. When reducing the distance of $Mg^+(3s)$ from the H—H bond the potential energy rises along a repulsve profile and the final plateau on the left now describes the strongly endothermic quasi-linear complex already apparent in Fig. 4. Such a complex formation gets energetically very close to the upper RPES, especially around the T-shaped geometries that nearly stabilize the excited state complex. The upper RPES profile in that same figure shows very clearly the occurrence of a much more strongly bound complex containing $Mg^+(3p)$: the new geometrical features of the valence electron density of the ion now strongly favour bond formation with H_2, especially at shorter distances where the bound $Mg^+(3p)$-H_2 comes very close to the lower surface. Another interesting feature on the upper RPES is the appearance on the left of a small barrier (slightly less than 0.2 eV) leading down to the insertion path at fixed H_2 distance (the one employed for the upper and lower curves of Fig. 7: 0.8 Å). The energy evolution of the linear configuration of the complex (the "insertion" complex) is given by the two cuts of the upper and lower RPES reported by Fig. 8. The data in that figure show variations of one of the Mg–H distances while the other (R_{opt}) was optimized at each value of the calculations. The energy profile on the lower surface clearly shows that, as one of the H atoms is moved away, the $MgH^+(X^1\Sigma^+)$ ionic molecule is formed. The $(H–Mg–H)^+$ complex at shorter distances shows the asymmetric nature of the bond with $Mg^+(3s)$: two different minima occur for the linear insertion, the latter also being an excited configuration (as shown by Fig. 2) with respect to the initial ionic species in the cold trap. On the other hand, the upper RPES cut in the same figure indicates again the marked energy stabilization for the complex with $Mg^+(3p)$ where the latter ion is coordinated to a "triplet" state of the H–H atoms. In other words, we see that both the T-shape and the linear insertion complexes exist on the upper surface as containing the two H atoms carrying the same spin density values (repulsive triplet state of the diatomic species) while the Mg^+ ion is now in its (3s) electronic state.

To further highlight the specific energy evolutions over both electronic states of the partners, we report in Fig. 9 a series of minimum energy paths (MEP) for the T-shape complex as a function of the R_x coordinate taken to be the distance of the Mg^+ from the mid-point of the H–H distance, the latter optimized in energy for each chosen R_x value. Several MEPs are reported in that figure in order to provide a more extensive comparison between the states involved. The following comments could be made:

- there is now a clear radial window where the two RPESs become closer to each other while forming T-shaped complexes,
- both the MEP_{ground} and $MEP_{excited}$ curves show the insertion-complex formation at R_x distances below about 1.4 Å. However, the lower MEP needs a substantial energy intake when going from the asymptotic $Mg^+ + H_2$ configuration on the extreme right of the figure to reach a nearly linear structure on the left. The upper MEP, on the other hand, shows a small endoergic effect when moving from the extreme right to the extreme left of its path.

Since the two "complex" arrangements correspond to different H–H distances, the two cuts discussed above are not really close in internal coordinate space and therefore we carried out two further levels of comparison which are given by the two additional curves reported by Fig. 9:

1. The curve marked E_{ground} describes calculations on the lower RPES but always using the H–H distances of the points of the upper RPES, in order to show two cuts in the same region in configurational space of the hydrogen molecule. We clearly see now that the lengthening of the H—H bond in the case of the $Mg^+(3s)$ partner ion in the lower RPES causes the strong energy increase discussed in the earlier figures: the two surfaces, however, now come very close to one another in the region where the transition can occur: between 1.4 and 1.8 Å of the R_x coordinate. In other words, the upper surface with $Mg^+(3s)$ combined with a "triplet" state of H_2 comes very close to the $Mg^+(3s)$ combined with a stretched vibrational state of $H_2(X^1\Sigma_g^+)$ in the lower RPES: this feature could therefore lead to efficient nonadiabatic crossings into the final products which are experimentally observed: MgH^+ and H atoms.
2. the dot-dashed curve reports the variations of the H–H distance along the previous path: it clearly shows the marked stretching of that bond as Mg^+ approaches it and the system moves to "insertion-type" configurations on both potential energy surfaces.

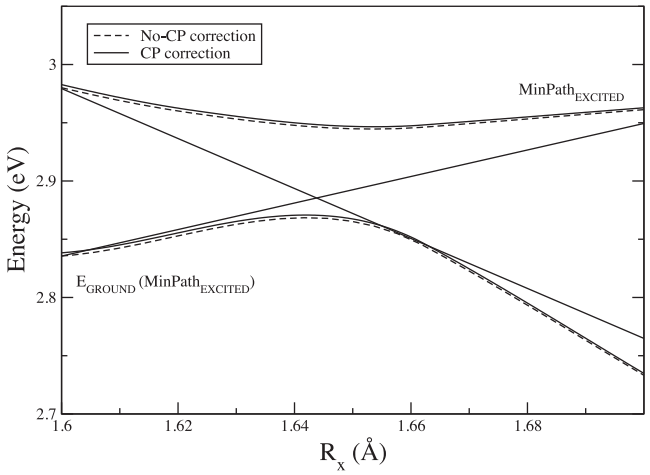

Fig. 10. Computed Minimum Energy Paths (MinPath) for the two electronic potential energy surfaces (with and without counterpoise correction) associated with the C_{2v} complex formations. The lower curves describe a strongly stretched $Mg^+(3s)\cdots H_2$ ($^1\Sigma_g$) while the upper, curves refer to the $Mg^+(3s)\cdots H_2$ ($^3\Sigma_u$) portion of the (2^2A_1) reactive surface. See main text for further details. The thin solid lines locate linear approximation to the crossing point and to the two slopes in that region.

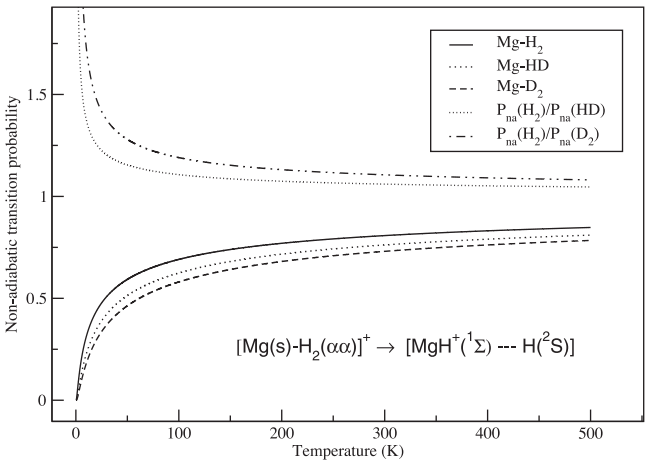

Fig. 11. Computed Landau–Zener nonadiabatic probabilities P_{na} for the products formations with different isotopologues of hydrogen molecules being uploaded in the trap. The ratios are reported by the upper two curves. See text for further details.

4. A simple 1D-modelling of the nonadiabatic coupling between RPESs

Our previous analysis has revealed the presence of at least two electronic configurations which are relevant for the interpretation of the events at the nanoscopic level: the $Mg^+(3p\ ^2P_{3/2})$ ion bound to the hydrogen molecule in a T-shaped structure on the upper RPES and the $Mg^+(3s\ ^2S_{1/2})$ bound to an $H_2(^3\Sigma_u^+)$ repulsive state. Thus, we have followed the energetic evolution of the partners on the (1^2A_1) ground state RPES in a weakly bound T-shaped complex [16] and the same partners on the more strongly bound complex on the upper (2^2A_1) excited RPES for the same T-shaped configurations [15]. Our calculations show them to come very close to one another in a region of potential energy surface crossing defined by the distance R_x between the Mg^+ ion (either 3s or 3p) and the mid bond of the H_2 ($^1\Sigma_g^+$) molecular partner. It corresponds to two different minimum configurations associated with different R_{H-H} distances within the C_{2v} complexes: $Mg^+(3s)\cdots H_2$ in the (1^2A_1) RPES [16] with R_{H-H} distances close to 1.4, and the strongly bound complex on the (2^2A_1) upper surface [15] with a stretched R_{H_2} distance. The data in Fig. 10 originate from our previous ab initio calculations that employed a highly correlated set of bound wavefunctions pertaining to the two relevant electronic states; the effect of the basis set superposition error (BSSE) in the region of the crossing has been evaluated via the counterpoise correction (CP) procedure and we found that the BSSE does not affect the shape of the two curves of Fig. 10, since a similar energy increase, of 1.6–2.8 meV is in fact observed for both the ground and excited states at the crossing. The upper RPES revealed that the excited Mg ion forms a strongly bound (10,750 cm^{-1}) complex of C_{2v} symmetry with a stretched H_2 ($^1\Sigma_g^+$) partner; it can evolve, on the same surface, to near-insertion configurations at the crossing region, where now the $Mg^+(3s)$ ion is forming a complex with a $^3\Sigma_u^+$ state (a "triplet" state) of the two hydrogen atoms that are bound to it.

The nonadiabatic crossing probabilities describe now the second step of a two-step reaction mechanism where the first one

$$Mg^+(3s)\cdots H_2(^1\Sigma^+g) \xrightarrow{h\nu} Mg^+(3p) - H_2(^1\Sigma_g^+) \quad (2)$$

occurs via laser pumping of the initial ion to its ($3p^2P_{3/2}$) electronic state.

The second step (on the upper RPES) involves moving without barrier to a different region of the latter, followed by a nonadiabatic transition to the products on the lower RPES

$$Mg^+(3p) - H_2(^1\Sigma_g^+) \longrightarrow Mg^+(3s) - H_2(^3\Sigma_u^+) \quad (3)$$

$$Mg^+(3s) - H_2(^3\Sigma_u^+) \xrightarrow{LZ} MgH^+(^1\Sigma^+) + H(^2S) \quad (4)$$

We could therefore model the evolution to products via a simple one-dimensional (1D) Landau–Zener (LZ) scheme which leads to MgH^+ being only weakly bound to an extra H atom. The latter can now leave the complex through redistribution of the energy gain caused by formation of the MgH^+ after the LZ process. The corresponding probabilities for the nonadiabatic transitions could be obtained using the well known Landau–Zener formula [30–33] in 1-D:

$$P_{na} = \exp(-\pi F_{na}) \quad (5)$$

$$F_{na} = \frac{\Delta E_{12}^2}{2\Delta F_{12} \cdot v} \quad (6)$$

where ΔE_{12} is the energy gap at the crossing, ΔF_{12} the difference in slope values at the same crossing, and v is the velocity that was taken to be essentially that of either D_2, H_2 or HD from the effusive uploading into the trap (~290 K [12]). The temperature dependence spanned in our calculations a broad range of possible trap values [6,12].

The following information can be gathered from the analysis of the probabilities given by Fig. 11:

1. from the low-T onset of the three P_{na} formation probabilities we see that such quantitites grow very rapidly, the one for H_2 reaching 50% of its final yield around 20 K of reaction temperature and growing to larger values as T increases. This means that each crossing is really efficient and that, given the large number of single crossings likely to occur during the permanence of the partner in the trap [12], one can consider the return of the "complex" to the lower RPES after the pumping as a very efficient reaction step;
2. the ratio between transition probabilities for the two processes associated with the uploading of either H_2 or D_2 (dashed-dotted upper curve) indicates that its values are remarkably close to

the experimental value of 1.5±0.4 [12]: since the plot shows a nearly constant value of about 1.2 from 100 to 400 K. These findings indicate that our suggested mechanism of H/D ejection after bond formation of either MgH^+ or MgD^+, one chiefly based on velocity differences between colliding partners, seems to provide a realistic description of the experiments;

3. the corresponding probability ratio in the case of either H_2 or HD uploading was found by the experiments [12] to be around 1.27±0.17. We have obtained the values given by the dotted curve, which yield a nearly constant ratio of about 1.20 when above 100 K of temperature, by considering the following equations:

$$\begin{aligned} &(A)\quad Mg(^2P_{3/2}) + H_2 \xrightarrow{\eta^{H_2}_{MgH^+}} MgH^+ + H \\ &(B)\quad Mg(^2P_{3/2}) + HD \xrightarrow{\eta^{HD}_{MgH^+}} MgH^+ + D \\ &\qquad\qquad\qquad\quad \xrightarrow{\eta^{HD}_{MgD^+}} MgD^+ + H \end{aligned} \tag{7}$$

where $\eta^{M'}_{M^+}$ is the probability of forming M^+ from M'. Hence the reaction probability of reaction (A) is $\eta^{H_2}_{MgH^+}$, and of reactions B is $\eta^{HD}_{MgH^+} + \eta^{HD}_{MgD^+}$. The probabilities ratio of reactions (A) and (B) is equal to the inverse of the sum of $\eta^{HD}_{MgH^+}/\eta^{H_2}_{MgH^+}$ and $\eta^{HD}_{MgD^+}/\eta^{H_2}_{MgH^+}$ of Fig. 3 of [12]. The values reported in Fig. 11 are fairly close to experiments over the whole range of temperatures. This indicates again that the crossing features employed within a simple LZ picture are providing a rather realistic modeling in relation to experiments.

4. the agreement found by our simple estimates and the experimental values therefore, suggests that in the present instance the isotopic effect is likely to be stemming from dynamical features rather than involving the more common tunneling path: the transition to the lower RPES causes an $(MgH/D)^+$ formation only weakly bound to either D or H, thus favoring the energy recovered from the newly formed ionic bond be redistributed into ejection of the extra H/D atom. Hence, this process is easier for the lighter atom with larger zero-point energy and becomes controlled by the relative velocities of the partners during the LZ transitions depicted by Fig. 10 and in line with the previous discussion.

5. Conclusions

The detailed analysis of the different cuts for the RPESs of the present work allows us to propose a possible nanoscopic mechanism which deal with $Mg^+(3s)$ and $H_2(^1\Sigma_g^+)$. As qualitatively suggested already by the experimental papers [6,7,12,13], our calculations confirm that process to be, broadly speaking, a multistep process:

- at the outstart, the $Mg^+(3s)$ undergoes laser pumping to its $Mg^+(3p)$ state, then interacts with the uploaded H_2, near thermal, molecules by forming a bound complex of T-geometry with a bond-stretched hydrogen molecule;
- the upper RPES complex undergoes a marked lengthening of the H_2 partner to ~4 Å, i.e. to some excited vibrational state of $H_2(^1\Sigma_g^+)$;
- the latter complex ion then evolves, without a barrier, over the upper RPES to a new, nearly linear insertion complex where the electron spin densities within the H partners describe a "triplet", repulsive state of the H_2 molecule ($^3\Sigma_u^+$) bound to the $Mg^+(3s)$ electronic state;
- that upper electronic configuration was shown by our calculations to occur in a region closely placed near the electronic state describing a weakly bound, lower complex of $[H^{\alpha}\text{-}Mg^{\beta}(3s)\text{-}H^{\alpha}]^+$, also with a "triplet" spin state of the two H atoms in the complex. Nonadiabatic transitions can therefore occur with fairly large efficiency in this region of geometries, thereby causing $MgH^+(X^1\Sigma)$ formation with a close-by extra H/D atom: the extra energy provided by the MgH^+ bond formation could in turn get redistributed within the new complex and rapidly eject the H atom weakly bound to newly formed MgH^+. Our simple energy redistribution mechanism also explains the larger rates seen for the deuterated product when compared to hydrogenic partners [12]: they are due to mass effects on the kinematics of the nonadiabatic process rather than to an alternative H-tunneling mechanism.

In conclusion, our present calculations for the electronic features of the two RPESs involved, plus a simple 1-D analysis of the non-adiabatic mechanisms between them, indicate that the overcoming of the strong endoergic nature of the MgH^+ formation from atomic ions can occur by coupling at least two electronic states where the Mg^+ ions are temporarily bound with either singlet or triplet states of H_2, the latter case allowing, by nonadiabatic transitions, the return of the Mg^+ ion to its $Mg^+(3s)$ state that forms a stable bond with one of the H atoms of an H_2 partner which now described to be in its dissociative "triplet" state.

Our present calculations, in spite of the average quality of our electronic basis set expansion choice (limited by the large number of configuration points we had to consider for our extended RPESs) have therefore established rather clearly the formation of an $Mg^+(3p)$ - $H_2(^1\Sigma_g^+)$ complex on the upper surface which then evolves along a short, barrierless path to another C_{2v} configuration on that upper surface, identified as an $Mg^+(3s)\cdots H_2(^3\Sigma_u^+)$ complex. The latter turns out to be very close to the lower RPES, which can then be efficiently reached via a simple 1-D Landau–Zener-type nonadiabatic transition. Its probability ratios given by our calculations turn out to be in good accord with experiments, thus providing for the first time realistic links between a simple quantum modeling of the reaction and its experimental features.

Acknowledgements

The computational support of an ISCRA HPC grant at the CINECA consortium is gratefully acknowledged. The CASPUR Supercomputing centre is also acknowledged for computational support. One of us (S.B.) thanks the CINECA Consortium for the awarding of an ISCRA Research Fellowship during which the present work was carried out.

References

[1] F. Lang, K. Winkler, C. Strauss, R. Grimm, J.H. Denschlag, Physical Review Letters 101 (2008) 133005.
[2] O. Dulieu, R. Krems, M. Weidemuller, S. Willitsch (Eds.), Physics and chemistry of cold molecules, Physical Chemistry Chemical Physics 13 (2011) 18703.
[3] Special issue on Cold molecules, Journal of Physics B, 39 (2006).
[4] F.A. Gianturco, M. Tacconi, Faraday Discussions 142 (2009) 463.
[5] X. Tong, D. Wild, S. Willitsch, Physical Review A 83 (2011) 023415.
[6] K. Mølhave, M. Drewsen, Physical Review A 62 (2000) 011401(r).
[7] S. Willitsch, M.T. Bell, A. Gingell, T.P. Softley, Physical Chemistry Chemical Physics 10 (2008) 7200.
[8] A. Bertelsen, S. Jørgensen, M. Drewsen, Journal of Physics B 39 (2006) L83.
[9] R. Wester, Journal of Physics B 42 (2009) 154001.
[10] J.C.J. Koelemeij, B. Roth, S. Schiller, Physical Review A 76 (2007) 023413.
[11] e.g. see: D. Gerlich, Physica Scripta, T59, 256, (1995) for further references.
[12] P.F. Staanum, K. Hojbjerre, R. Western, M. Drewsen, Physical Review Letters 100 (2008) 243003.
[13] M. Drewsen, I. Jensen, J. Lindballe, N. Nissen, R. Martinussen, A. Mortensen, P. Staanum, D. Voigt, International International Journal of Mass Spectrometry 229 (2003) 83.

[14] M.W. Schmidt, K.K. Baldridge, J.A. Boatz, S.T. Elbert, M.S. Gordon, J.H. Jensen, S. Koseki, N. Matsunaga, K.A. Nguyen, S.J. Su, T.L. Windus, M. Dupuis, J.A. Montgomery, Journal of Computational Chemistry 14 (1993) 1347–1363.
[15] C.W. Bauschlicher Jr., Chemical Physics Letters 201 (1993) 11.
[16] V. Dryza, E.J. Bieske, A.A. Bucachenko, J. Klos, Journal of Chemical Physics 134 (2011) 044310.
[17] C.W. Bauschlicher, H. Partridge, Chemical Physics Letters 181 (1991) 129.
[18] V. Dryza, B.L. Poad, E. Bieske, Journal of Physical Chemistry A 113 (2009) 199.
[19] A.J. Page, D.J.D. Wilson, E.I. von Nagy-Felsobuki, Physical Chemistry Chemical Physics 12 (2010) 13788.
[20] M. Tacconi, F.A. Gianturco, European Physics Journal D 54 (2009) 31.
[30] L.D. Landau, Physikalische Zeitschrift der Sowjetunion 2 (1932) 46.
[31] C. Zener, Proceedings of the Royal Society A 137 (1932) 696.
[32] R.E. Olsen, F.T. Smith, Physical Review A 3 (1971) 1607.
[33] H. Nakamura, Journal of Chemical Physics 87 (1987) 4031.